ANL-98/11

Argonne National Laboratory

Metallic Uranium ZPPR Fuel: Corrosion Characteristics and Corrosion Product Oxidation Kinetics

by

T. C. Totemeier, R. G. Pahl, S. L. Hayes, and S. M. Frank

Argonne National Laboratory, Argonne, Illinois 60439
operated by the University of Chicago
for the United States Department of Energy under Contract W-31-109-Eng-38

DISCLAIMER

Reproduced from the best available copy.

Available to DOE and DOE contractors from the
Office of Scientific and Technical Information
P.O. Box 62
Oak Ridge, TN 37831
Prices available from (423) 576-8401

Available to the public from the
National Technical Information Service
U. S. Department of Commerce
5285 Port Royal Road
Springfield, VA 22161

Distribution Category: UC-504
Materials

ANL-98/11

ARGONNE NATIONAL LABORATORY
P.O. Box 2528
Idaho Falls, Idaho 83403

Metallic Uranium ZPPR Fuel: Corrosion Characteristics and Corrosion Product Oxidation Kinetics

by

T.C. Totemeier, R.G. Pahl, S.L. Hayes, and S.M. Frank

Engineering Division
Argonne National Laboratory - West

October 1997

TABLE OF CONTENTS

LIST OF FIGURES

LIST OF TABLES

Metallic Uranium ZPPR Fuel: Corrosion Characteristics and Corrosion Product Oxidation Kinetics

by

T.C. Totemeier, R.G. Pahl, S.L. Hayes, and S.M. Frank

PREFACE

This report presents the findings of a characterization of corroded highly enriched uranium (HEU) fuel plates used in the Zero Power Physics Reactor (ZPPR) and preliminary results obtained on the oxidation kinetics of corrosion products formed on the plates. The body of the report is divided into two parts. The first part details the history of the corroded ZPPR plates and their specific corrosion characteristics. The second part summarizes the results of initial oxidation tests on hydride-containing corrosion products from a single fuel plate. The results of measurement of the corrosion product specific surface areas are also presented in the second part. Tables, figures, and references are given at the end of each part.

PART 1
THE ZPPR FUEL EXPERIENCE: A CASE HISTORY OF URANIUM CORROSION IN EXTENDED STORAGE

I. INTRODUCTION

Interest in the long-term storage properties of uranium metal has been renewed in recent years due to the extended underwater storage of metallic spent nuclear fuels (SNF) and the anticipated interim to long-term dry storage of SNF and uranium metal feedstock. Metallic SNF currently of concern include N-reactor, EBR-II, and Fermi. The principal concern with storage of uranium metal fuels is degradation due to oxidation and corrosion during the storage period, and the possibility of forming reactive corrosion products, such as metallic fines or uranium hydride (UH_3) powder. Formation of reactive corrosion products presents safety hazards when handling the material after storage. Early anecdotal evidence on the hazards of handling improperly stored uranium was documented by Smith in 1956 [1].

Since that date, the reaction of uranium with oxygen and water vapor have been fairly extensively studied; two detailed reviews have been published by Colmenares [2, 3]. Uranium reacts fairly slowly with dry air or dry oxygen, forming an initially passive layer of slightly superstoichiometric UO_2. Diffusion of oxygen ions through the passive layer is rate controlling; cracking of the oxide at greater thickness limits its protective abilities. The reaction of uranium with water vapor also produces UO_2, according to the formula:

$$U + 2\,H_2O \rightarrow UO_2 + 2\,H_2 \qquad (1\text{-}1)$$

This reaction occurs at a much greater rate than the uranium-oxygen reaction. It is generally found that less than the stoichiometric amount of hydrogen gas is formed in this reaction; most researchers report the presence of UH_3 to account for the remainder of the hydrogen. The reported values of the percentages of UH_3 in the nominally oxide reaction product vary from 2% to 30% [4-6]; the exact mechanism of hydride formation is still under debate. Instances of higher percentages formed in corrosion products have been limited to crevice-type corrosion where there is limited access of the ambient environment to the reaction product. In such a situation trapped hydrogen may react with the metal directly to form hydride.

UH_3 forms as a fine powder, is reported to be pyrophoric in the presence of air [7], and can burn at room temperature according to the relation:

$$UH_3 + \frac{7}{4} O_2 \rightarrow UO_2 + \frac{3}{2} H_2O \qquad (1\text{-}2)$$

This reaction liberates a significant amount of heat, 1,386 kJ/mol UH_3. Uranium metal fines may also be produced as a result of corrosion—these will also oxidize very rapidly at room temperature in air and generate heat. As uranium products are removed from enclosed storage situations where hydride and/or metal fines may have formed, exposure of the corrosion products to air may result in pyrophoric incidents, or in some cases even burning of the bulk metal itself [1].

Few reports currently exist in the literature documenting instances where hydride has been found as a corrosion product of metal after extended storage. The corrosion in storage of highly-enriched uranium (HEU) fuel plates manufactured for use in the Zero Power Physics Reactor (ZPPR) at Argonne National Laboratory (ANL) provides one such example. These plates are coupons of HEU clad in stainless steel; crevice corrosion of the plates has occurred since they were originally clad in 1982. A detailed characterization of the plates and their corrosion products is currently being performed to gain more knowledge of the nature of uranium corrosion, and also as an initial step towards examination of metallic SNF from the Experimental Breeder Reactor-II (EBR-II) which is currently in wet storage.

This part details the history of the ZPPR fuel plates and the results of an initial characterization of the corrosion and the corrosion products. The background relating the reasons for cladding the plates, the initial observations of corrosion, and the attempts to halt corrosion are first presented. The current state of the plates and corrosion characteristics are then described, followed by a numerical analysis of potential pyrophoric events in handling the plates. Finally, actual handling and passivation experience with the plates are presented.

II. HISTORICAL BACKGROUND

A. Plate Production and Early Experience

The Zero Power Physics Reactor (ZPPR—originally termed the Zero Power Plutonium Reactor) began operation in 1969. It was built to provide a testbed for fast-critical assembly reactor physics experiments in support of advanced fast reactor designs, and was the culmination

of a series of fast critical facilities—ZPR-3, ZPR-6, and ZPR-9. The ZPPR reactor provided the capability to mock-up many fast-critical power reactor configurations and perform reactor physics measurements while operating at an extremely low power (less than two kilowatts). Most ZPPR fuel elements are stainless steel containers that are loaded with rectangular pieces of reactor materials. Many types of reactor materials were available for use, including highly enriched uranium (HEU) metal.

The HEU plates which were used in the ZPPR reactor were originally manufactured for use in the earlier ZPR reactors. The manufacture of the first HEU plates for use in ZPR-3 was described in 1955 by Yaggee [8]. These plates were 7.64 cm (3 inches) by 5.08 cm (2 inches) by 3.18 mm (1/8 inch) in dimension, and were produced by hot rolling cast billets of uranium. The rolled sheet was sheared, stamped, and machined to close final dimensional tolerances. References in this document and others are made to earlier plates manufactured by Sylvania Electric Products through a hydride-dehydride powder metallurgy (PM) process. The rolling operation was chosen over the powder metallurgy process to meet a production deadline. HEU plates 1.59 mm (1/16 inch) thick were also used in the ZPPR reactor. No information detailing their manufacture has been found, but it is known that they were produced through a rolling process.

ANL memoranda from 1961 describe the "crumbling" of some of the HEU plates, all of which were manufactured by Sylvania using the PM route. It was determined that the plates were deteriorating due to slow oxidation within porosity present in the plates; the porosity was a result of improper processing. J.G. Schnizlein performed ignition tests on samples from deteriorated plates [9]. The ignition temperature was measured to be 115°C, compared to 480°C for unaffected material. The deteriorated plates represented a clear pyrophoricity hazard and were stored in an inert atmosphere in sealed paint cans buried in sand. None of the plates manufactured using the PM process were used in the ZPPR reactor.

All of the ZPPR plates originally were coated with a non-hydrogenous, organic polymer coating, C_2F_3Cl, commonly referred to as KEL-F. This coating was applied to prevent spread of contamination, and to retard oxidation of the plates during their exposure to the ambient environment. Apparently this coating was not fully effective in preventing oxidation, as the plates—some described as "badly oxidized"—were re-coated in 1969.

In 1981, the decision was made to remove the KEL-F coating and place the plates into stainless-steel cladding. The prime motivator for use of a cladding was elimination of alpha contamination. The ZPPR reactor also used a U-Pu-Mo alloy as a fuel material. Plates of this

alloy were clad in sealed stainless-steel jackets. One way of detecting breaches in the jackets was by detecting alpha contamination. The HEU plates coated with KEL-F commonly spread alpha contamination by scraping and abrasion: this contamination could not be readily distinguished from contamination arising from a U-Pu-Mo jacket breach. Cladding the HEU plates eliminated this extra source of alpha contamination.

The cladding operation was performed from February 1982 through January 1983. The KEL-F coating was removed by dissolution in a butyl acetate solvent with two rinse steps, also in butyl acetate. After the final rinse, the plates were dried in a wire rack and inserted into a 125 μm thick type 304 stainless steel cladding jacket. The stainless steel cladding was sealed at each end by a porous metal frit end plug. The porous end plugs were specifically chosen to allow any residual organic vapors to escape from inside the cladding and to allow the plates to "breathe". Subsequent experience revealed this decision to only worsen the corrosion problem.

At this point, the terminology that will be used to describe the plates should be clarified. For the purposes of this report, "coupon" will refer to the rectangular HEU metal pieces themselves, while "plate" will refer to a stainless-steel clad assembly of one or more "coupons". Figure 1-1 is a schematic diagram showing a clad assembly of plates. As described above, as-manufactured coupons came in different lengths and thicknesses; all coupons were 51 mm (2 inches) wide. The two available lengths were 51 mm (2 inches) and 76 mm (3 inches); 3.2 mm (1/8 inch) and 1.6 mm (1/16 inch) thicknesses were available. These coupons were assembled into clad plates with lengths varying from 51 mm (2 inches) to 203 mm (8 inches). The plates have been, and are currently, stored in the ZPPR vault in rectangular aluminum overpack canisters which have rubber gasket seals.

B. Initial Observations of Clad Plate Corrosion

Corrosion of the plates was first noticed in 1985, only three years after the cladding operation. The plates were required to meet a dimensional specification for use in the ZPPR reactor, and at this time several plates did not meet the specification due to outward bulging of the cladding. Figure 1-2 is a photograph from 1985 showing plates in an overpack canister; bulges can be observed on the plate edges. To determine the nature of the bulging, four defect plates were sent to the ANL-W analytical laboratory for examination.

The plates were declad by filing along their edges and peeling back the cladding to expose the HEU coupons. The operation was performed in an air hood, and when the cladding was

peeled back from a particularly bulged area of one plate, a strong flash was observed. Figure 1-3 shows the plate, after decladding, for which the flash was observed. Of the three coupons, one was severely corroded, and a substantial amount of powder remained in the cladding. X-ray diffraction of corrosion products from the four plates showed the presence of UO_2, both α and β forms of UH_3, and UN. The observation of pyrophoric events during decladding was attributed to the presence of UH_3 in the corrosion product. After examination, the plates were cleaned with nitric acid and returned to ZPPR. Further details of the corrosion characteristics are presented in Section III.

The observation of pyrophoric events and UH_3-containing corrosion products resulted in a decision to identify actions sufficient to inhibt continued corrosion of the plates. The corrosion itself was thought to be initiated by moisture entering edge cracks in the coupons prior to cladding, and perpetuated by continuing moisture access to the coupons via the porous metal end-caps. The first remedial action was to place bags of anhydrous $Mg(ClO_4)_2$ desiccant in the overpack canisters with the plates. The desiccant was intended to remove moisture from the ambient atmosphere in which the plates were stored.

In 1990, continued corrosion was observed in the form of additional plates being dimensionally rejected due to bulging. A study determined that the anhydrous $Mg(ClO_4)_2$ did not act as an effective desiccant because of the reversibility of $Mg(ClO_4)_2$ hydration; uranium was determined to have a greater affinity for water than $Mg(ClO_4)_2$. Another attempt to halt corrosion was made by evacuating the overpack canisters. The canisters were fitted with a vacuum port to accommodate this measure.

Unfortunately, the canisters were not originally designed for evacuation; the upper and lower halves of the canister were joined by only two bolts, one at each end. Most canisters leaked sufficiently to allow a return to atmospheric pressure fairly quickly. The storage procedure called for yearly inspection of the canisters and re-evacuation if necessary, which only exasperated the corrosion problem. Once air leaked into the canister, O_2 and H_2O would react with U in the plates, causing a pressure differential which permitted further air in-leakage and further oxidation, the final canister environment theoretically being mostly nitrogen at nearly atmospheric pressure. At that point oxidation of the plates should have stopped. Re-evacuation of the canisters simply re-initiated the above cycle by renewing the pressure differential.

This cycle of continuing corrosion was confirmed in 1992 by analysis of the gas present in the canisters about a year after evacuation [10]. Five canisters were studied: two containing plates

already rejected by excessive bulging, and three containing plates that were considered to be in "good" condition. The pressure in four of the five canisters was nearly at atmospheric levels, confirming that leakage had occurred. The pressure in the fifth canister was approximately one-third of atmospheric. The oxygen content in all canisters had been reduced to less than one volume percent, and hydrogen levels were high, ranging from 0.16 vol.% to 13.34 vol.%. The conclusion was that oxidation by O_2 and H_2O had occurred, even in canisters with good plates.

In this same period, a second examination of a reject plate was performed. A bulged plate was de-clad in a fume hood. A loose black powder was found in the cladding, and the uranium coupons were visibly oxidized. Upon wire brushing of the de-clad uranium plate, a colorless flame erupted and burned. The black powder which had been separated from the plate but was in the same container also ignited. The fire was quickly extinguished with Metal-X powder. Burning of the powder confirmed what was suspected about the corrosion product—it contained a significant quantity of uranium hydride along with uranium oxide, and the hydride was easily ignited in air.

As a result of these findings, evacuation of the canisters was discontinued. At the same time, a search was conducted to find an appropriate getter to remove reactive gases from the overpack canisters. The getter which was chosen for use was a packet containing unsaturated hydrocarbon with a palladium catalyst and lithium hydride. The hydrocarbon is 1,4-bis (phenylethynyl) benzene (referred to as "DEB"), which contains two carbon-carbon triple bonds. The getter removes hydrogen, water vapor, and oxygen via the following reactions:

$$2H_2 + O_2 \rightarrow 2\ H_2O \text{ (via Pd catalyst)} \qquad (1\text{-}3)$$

$$H_2O + LiH \rightarrow LiOH + H_2 \qquad (1\text{-}4)$$

$$2H_2 + (-\ C \equiv C-\ ) \rightarrow (-\ CH_2 - CH_2\ -) \text{ (via Pd catalyst)} \qquad (1\text{-}5)$$

Reaction (5) is irreversible. The lithium hydride material is present to scavenge any water vapor present in the environment or any produced by reaction (3). The Pd is needed to catalyze the reaction of hydrogen with the DEB material.

The getters were used by placing a getter packet in the overpack canisters and then backfilling each canister with dry nitrogen gas. The gas in several canisters was sampled each month and checked for oxygen and hydrogen. No concentrations in excess of 0.1 volume percent were observed. In addition, yearly inspection of the canisters containing useable plates has

revealed no additional rejects since the use of the getters. Unfortunately, over the course of the 12 year time period from the cladding operation to the use of getters over 25 percent of the total plate inventory underwent sufficient corrosion to be rejected, an amount which corresponds to over 2000 plates.

C. Current Status

The ZPPR HEU plates are currently stored in overpack canisters containing getters in the ZPPR vault. The ZPPR reactor itself is in non-operational standby. The reject plates are being processed (see Section IV below) to supply Babcock & Wilcox (B&W) HEU for research reactor fuel production. The reject plates are considered a uranium storage vulnerability and will be processed in the future to stabilize the corrosion products.

III. CORROSION CHARACTERISTICS

A. Morphology

Corrosion of the uranium coupons manifests itself in the clad plates as extensive bulging of the cladding. Distortion of the cladding edges is apparent in Fig. 1-2. Figure 1-4 shows a single plate with extensive cladding deformation along the two long edges of the plate. The insert close-up in Fig. 1-4 shows a significant breach which has occurred due to cladding deformation. The bulges were most commonly found along the edges of the cladding, rather than in the center. Severe localized corrosion attack was correspondingly found to initiate along the edges of the uranium coupons, as described below. The cladding itself showed no sign of corrosion attack; the cladding breach appears to have been solely due to the volume expansion of the corrosion product relative to the parent metal. For uranium metal being transformed to the dioxide, a minimum expansion of 72% occurs. A wide range of bulging and deformation was observed among the "reject" plates. Some plates showed very little sign of bulging, while others were grossly deformed with more than one cladding breach.

The severe corrosion of the uranium coupons was clearly observed upon de-cladding of the plates. Loose powder and dust quickly spread throughout the work area. In the most recent characterization activity, all de-cladding of plates was carried out in a glovebox containing a pass-through Ar atmosphere. Figures 1-3 and 1-5 show coupons immediately following cladding removal. Figure 1-3 is an archival photo from 1985, and Fig. 1-5 is a recent photo showing the coupons from the bulged plate of Fig. 1-4. A clear difference between the two coupons was the

extent of general corrosion. The coupons in Fig. 1-5 showed a large amount of general corrosion which was manifested in the form of gray flakes and fine dust. Much of the gross corrosion product was removed from these coupons before photographing them. In contrast, little general corrosion was observed for the coupons in Fig. 1-3; especially for the two coupons on the left side.

A second form of corrosion observed was more severe and localized. This type of corrosion is clearly shown on the right hand side coupon in Fig. 1-3 and the top coupon in Fig. 1-5. This form of corrosion had several notable characteristics. First, localized corrosion was almost always observed on only a single coupon for each plate (a given plate contains two or three coupons). The corrosion appeared to have initiated at the transverse edges of the coupons, and often took the form of plate blistering or transverse cracking. Figure 1-6 shows a coupon with severe cracking and blistering attack (photo taken after loose corrosion product removal), while the right hand plate in Fig. 1-3 shows lifting of metal due to sub-surface cracking and attack. Cracking and blistering were most commonly observed at early stages of corrosion (judging on the basis of overall attack). For more severely corroded plates a more general attack was observed, as shown in Fig. 1-5. In addition, no relationship between the presence of localized corrosion for a given coupon and location of the coupon within the plate was observed, *i.e.* it did not occur only for coupons adjacent to the endplugs.

The above characteristics suggest that the localized corrosion may be microstructurally related. Metallographic cross-sections of three corroded plates were prepared to further investigate the relationship between coupon microstructure and localized corrosion. The first plate was the severely corroded plate shown in Fig. 1-6, the second was a plate which showed moderate localized corrosion, and the third was a plate which did not show any localized corrosion. Due to the thickness of oxide on the plates, all three proved difficult to polish. During final polishing the oxide particles tended to separate themselves from the plates and scratch the metal surface. The first two plates which had localized corrosion showed interior cracking along the plates' longitudinal axis, as shown in Fig. 1-7. The first plate had many more cracks than the second. The third plate did not show any interior cracking. Unfortunately, no distinct microstructural features were identified which could account for the apparent increased susceptibility of some plates to localized corrosion compared to others. No highly elongated grains or oriented inclusions were observed in the plates with localized corrosion.

B. Products

The corrosion products from the plates were composed of two distinctly different types—a light gray, flake-like material, and a black powder. Fig. 1-8 is a photograph of the corrosion product obtained from the plate in Fig. 1-4. For this plate, which was considered to be relatively badly corroded, there were approximately equal volumes of flake and powder. Some of the powder was found agglomerated into fairly large chunks one or two millimeters in size. These chunks are easily broken into powder. The presence of large quantities of powder appeared to be related to the amount of localized corrosion present, i.e. the more localized corrosion, the more powder present in the corrosion product. In the de-cladding operation it was clear that the powder material was associated with areas of *local* corrosion. The corrosion product from plates which did not show severe bulging and localized corrosion were composed nearly entirely of flake material.

Samples of the two forms of corrosion product shown in Fig. 1-8 were analyzed using X-ray diffraction (XRD) to determine the phases present in each. All corrosion product XRD samples were crushed to a fine powder in a high-purity Ar glovebox and then loaded into an environmental chamber. XRD was performed on a Scintag X1 powder diffractometer using Cu K-alpha radiation. The scan range was from 20° to 100° 2θ with a scan rate of 0.75 degrees per minute.

Diffraction patterns in the 2θ range from 20° to 60° are shown in Fig. 1-9. The powder material was found to have strong β-UH_3 peaks, with small peaks of either UO_2 or U_3O_7 (UO_{2+x}). Both types of uranium oxide had a good match with the diffraction pattern. Due to the width of the peaks it was not possible to differentiate between the two. In contrast, the flake material showed strong peaks from the oxide and only minor hydride peaks.

A semi-quantitative XRD analysis was performed on samples from two additional plates. The first plate (referred to as the "bad plate") showed severe bulging and localized corrosion similar to the plate shown in Fig. 1-4, while almost no bulging was apparent on the second plate (referred to as the "good plate"). All of the loose corrosion product from each plate was collected by brushing the coupons with a stiff horsehair brush. This process left an adherent oxide film on the coupons. The loose corrosion product from each plate was ground into a single uniform powder. Diffraction was performed on a sample of this powder, in hopes of obtaining a pattern which was representative of an "average" of product from the plate as a whole. The diffraction patterns obtained were analyzed using Sietronics standardless quantitative XRD phase analysis

software. Using this technique, the UH_3 content of the loose powder from the bad plate was estimated to be approximately 80 wt.% with 20 wt.% oxide. The loose powder from the good plate was entirely oxide; no hydride peaks were observed.

C. SPARC Analysis

In an effort to evaluate the ignition hazard associated with the hydride-bearing, corroded fuel plates, a mechanistic model for uranium ignition developed previously by Totemeier and Hayes [11] was used to analyze the corroded ZPPR plates. This model, whose code is denoted "SPARC", predicts the ignition temperature of metallic uranium as a function of specific surface area. The uniqueness of this model is its ability to analyze ignition potential of a uranium metal substrate when UH_3-bearing surface films are present.

Based on the loose corrosion product weights described below in Section IV, a mass of ~6.6 g of loose corrosion product was present on a typical, badly corroded coupon that originally contained 75 g of uranium metal. The geometrically calculated specific surface area of a ZPPR fuel coupon is approximately 0.3 cm^2/g. The ignition model was used to analyze the room-temperature (300 K) ignition potential of such a coupon assuming that this amount of corrosion product was a film of uniformly mixed UO_2 and UH_3 evenly distributed upon the surface of the coupon.

With the further assumption that any UH_3 present in the corrosion product ignited spontaneously in air, SPARC analysis indicated that room temperature ignition of the uranium metal substrate would result if the UO_2-UH_3 corrosion product mixture contained at least 33% UH_3. Since the XRD analysis indicated that the hydride fraction in the loose corrosion product was in fact greater than this value, it was assumed that there was a high potential for ignition of the ZPPR fuel plates with the corrosion product unremoved. The analysis and conclusions are conservative because the hydride fractions determined by XRD do not account for adherent oxide remaining on the plates—actual hydride fractions will be lower.

IV. RECENT HANDLING EXPERIENCE

In 1995 Babcock and Wilcox (B&W) approached ANL-W to obtain HEU from the ZPPR plates for production of research reactor fuel. A processing sequence was proposed to produce HEU ingots for B&W; this processing would also serve as a stabilization method for the corroded plates. The plates were to be de-clad in an argon glovebox with a pass-through atmosphere containing between one and three percent oxygen. Exposure of the hydride-containing corrosion

product to a small level of oxygen was expected to passivate the hydride (by forming a layer of oxide) without risk of ignition. The plates and powder were to be loaded into a yttria-coated graphite crucible and transferred to an induction casting furnace. The furnace would be evacuated and the plates melted. Under this scenario, heating of the powder in a vacuum would decompose the hydride into metal, which would be incorporated into the rest of the melt. The resulting ingot would be broken into smaller pieces and shipped to B&W.

Based on previous experience with the plates and the numerical analysis detailed in Section III.C above, a concern about the proposed process was raised. During placement of the loaded crucible into the furnace, the plates and powder could possibly be exposed to air for a short period of time (approximately three minutes) before the furnace was closed and evacuated. Exposure to air could ignite the hydride if it were not fully passivated, which could in turn cause ignition of the underlying uranium metal. In view of these concerns, an experiment was initiated to determine whether the hydride was adequately passivated by its exposure to the oxygen-containing glovebox atmosphere.

The first experiment involved de-cladding four plates which were specifically selected as showing severe bulging but no cladding breaches. The plates were de-clad in a pass-through Ar glovebox by cutting the ends of the cladding off with a tin snips and peeling the cladding away from the uranium coupons. Significant quantities of corrosion product were present in the cladding. About 80 grams of corrosion product were present in the four plates which comprised approximately 900 grams of metal initially. The 12 de-clad uranium coupons and corrosion product were loaded into an open steel food-pack can and left to sit exposed to the glovebox atmosphere for two hours. The coupons were stacked like a deck of cards in the bottom of the can. The corrosion product completely covered the bottom few coupons; the rest were not in contact with the product, except for small amounts that clung to surfaces of the coupons. The can was bagged out of the glovebox and transferred to a closed-face air hood.

The bag was carefully removed in the hood and the contents of the can observed. No immediate visible reactions occurred. The can was picked up through glove-ports in the face of the hood—no heat was detected. The can was agitated by gently shaking—again no reaction was noted. Next, individual plates were flipped over using a flathead screwdriver. Nothing occurred for the first plates on the top of the stack. Striking the plates produced sparks, as has been typically in handling of uranium metal at ANL-W. As plates nearer to the bottom were handled and struck, areas of the powder approximately 10 mm in diameter began to flare. The appearance was that of a sparkler, with many fine sparks. A reddish-blue flame was also observed. Within about

five seconds of the start of powder ignition, the contents of the can were dumped into a flat-bottomed steel pan. The steel can holding the plates and powder had become noticeably warm (through a rubber glove) very quickly. Burning of areas of the powder (in the form of sparks) continued after dumping. Some areas of the powder, and metal in close contact with the powder, had reached an orange color.

At this point (maybe five seconds after reactions began), Metal-X was poured over the coupons and corrosion product. The reaction appeared to have been halted, but agitation of the product caused local re-ignition. Further application of Metal-X again stopped the reaction, which appeared to smolder under the Metal-X. One coupon was removed from the pan. A small piece of powder adhered to the metal and burned, scorching the underlying metal. No further reaction of that coupon occurred—striking the coupon to produce sparks did not result in a reaction. Once the reaction of the powder appeared to be complete (i.e. stirring of the powder–Metal-X mixture did not cause reaction), all of the coupons were separated from the powder. Some appeared slightly scorched, but none could be made to further react.

The conclusion of this experiment was that simple exposure of the corrosion product to the 2% oxygen glovebox atmosphere for two hours was not sufficient to fully passivate the uranium hydride in the corrosion product. It was also determined that the metal coupons alone would not react. Hence in subsequent operations the coupons were separated from the powder. Further experimentation was needed to determine passivation conditions for the separated powder.

For the second experiment, 36 ZPPR plates which were considered to be typical of the reject plates were de-clad in the pass-through glovebox. As each plate was de-clad, the corrosion product was removed from the individual coupons using a paintbrush. The coupons were loaded into the crucible; the powder and flakes were collected in a steel can. The second batch of plates were much less corroded than the first. On average, only approximately 1.5 grams of corrosion product was found per plate, about 80 grams total from 8 kg of uranium. As the powder and flakes accumulated, they were transferred to a mortar and pestle, ground to a fine powder, and spread out in the bottom of a steel pan. The depth of the powder bed was approximately two millimeters. The powder was then allowed to sit undisturbed in an Ar-2%O_2 atmosphere for two hours at room temperature.

An 8 gram sample of the powder was then placed in a plastic bottle, bagged out, and transferred to the air hood. The bag was removed and the powder quickly poured into a steel pan. No reaction was observed. The powder was successively agitated by shaking, stirring, light

pounding with a hammer and finally by grinding. There were no signs of any reactions; the powder appeared to have been completely passivated. The remainder of the powder in the pass-through glovebox was transferred to the hood and treated in a similar fashion. Again, no reactions were observed.

The conclusion of the second experiment was that the operation of grinding the corrosion product flake and powder to a fine powder using the mortar and pestle sufficiently exposed the hydride to the 2% oxygen-containing glovebox atmosphere to convert the majority of it to oxide, such that no further reaction occurred in air. The crucible containing the metal coupons was transferred to the casting furnace; the casting was successfully performed without incident.

This procedure was adopted for use in further passivation operations. As of May 1997, approximately 1200 plates have been processed using this procedure and 315 kg of HEU metal has been supplied to B&W. No pyrophoric incidents occurred during this time period. The passivated corrosion product is currently being stored in sealed foodpack-type cans in the FMF vault; this material will eventually be further passivated by heating to a high temperature in air.

V. CONCLUSIONS

This part summarized the past experience at ANL-W with uranium metal ZPPR fuel plates and presented descriptions of the corrosion morphology and corrosion product characteristics. The ZPPR plates have a long history of corrosion problems, which became more serious following cladding of the plates using porous metal endplugs. The restriction of oxygen by the cladding presence resulted in the formation of significant quantities of uranium hydride; the presence of uranium hydride in the corrosion product was confirmed using XRD. Analysis of the corroded ZPPR plates using a numerical ignition model identified a potential room temperature ignition hazard. Past and recent handling experience with the plates has demonstrated both the potential for pyrophoric events and one procedure for mitigating these events.

REFERENCES

[1] R.B. Smith, The Fire Properties of Metallic Uranium (TID-8011) (Technical Information Service - Atomic Energy Commission, Washington D.C., 1956).

[2] C.A. Colmenares, Prog. Solid State Chem. 9 (1975) 139.

[3] C.A. Colmenares, Prog. Solid State Chem. 15 (1984) 257.

[4] T. Kondo, F.H. Beck, and M.G. Fontana, Corrosion 30 (1974) 330.

[5] M.M. Baker, L.N. Less, and S. Orman, Trans. Faraday Soc. 62 (1966) 2513.

[6] K. Winer, C.A. Colmenares, R.L. Smith, and F. Wooten, Surface Science 183 (1987) 67.

[7] J.J. Katz and E. Rabinowitch, The Chemistry of Uranium - Part I (McGraw-Hill, New York, 1951).

[8] F.L. Yaggee, The Manufacture of Enriched ZPR-III Fuel Plates, Argonne National Laboratory Report ANL-5599 (1956).

[9] J.G. Schnizlein, Ignition Properties of Certain ZPR-III Blanket Plates, Argonne National Laboratory Internal Memorandum to R.C. Vogel, March 16, 1961.

[10] C.W. Solbrig, J.R. Krsul, and D.N. Olsen, Proc. DOE Spent Nuclear Fuel – Challenges and Initiatives, Salt Lake City, UT, Dec. 13-16, ANS, La Grange Park, IL, 1994.

[11] T.C. Totemeier and S.L. Hayes, Proc. DOE Spent Nuclear Fuel and Fissile Material Management, Reno, NV, June 16-20, ANS, La Grange Park, IL, 1996.

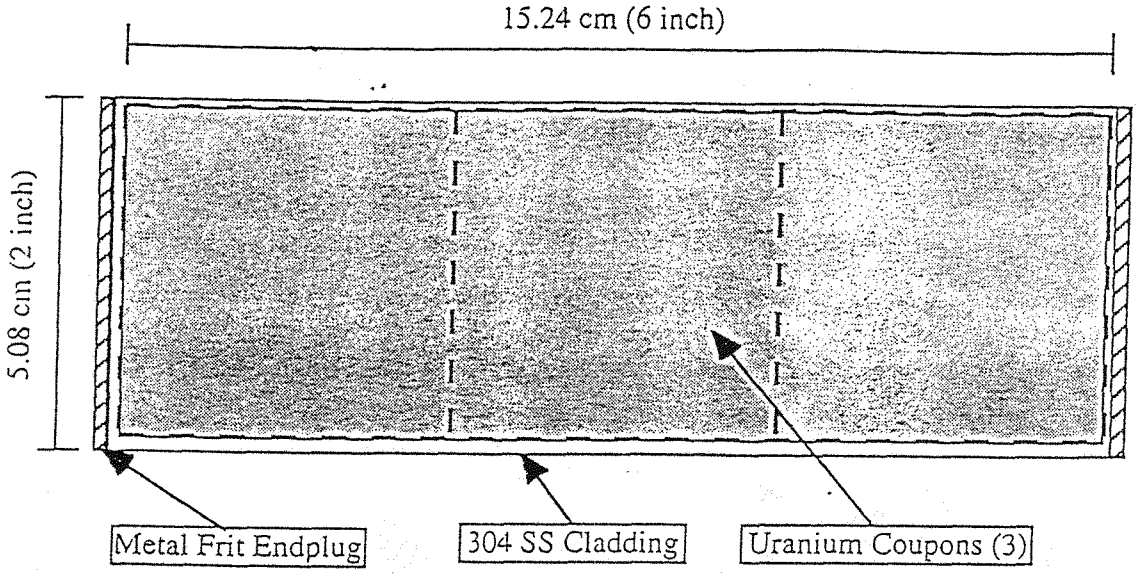

Figure 1-1. Schematic diagram of ZPPR Plate and Coupons.

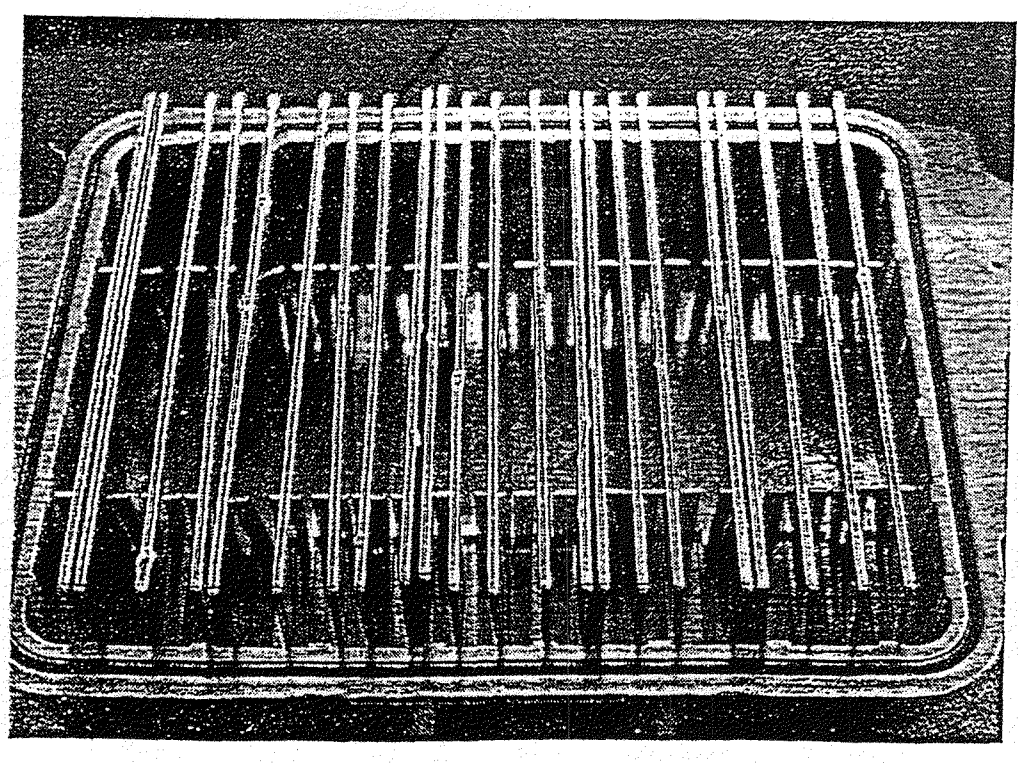

Figure 1-2. Bulged ZPPR plates in overpack canister.

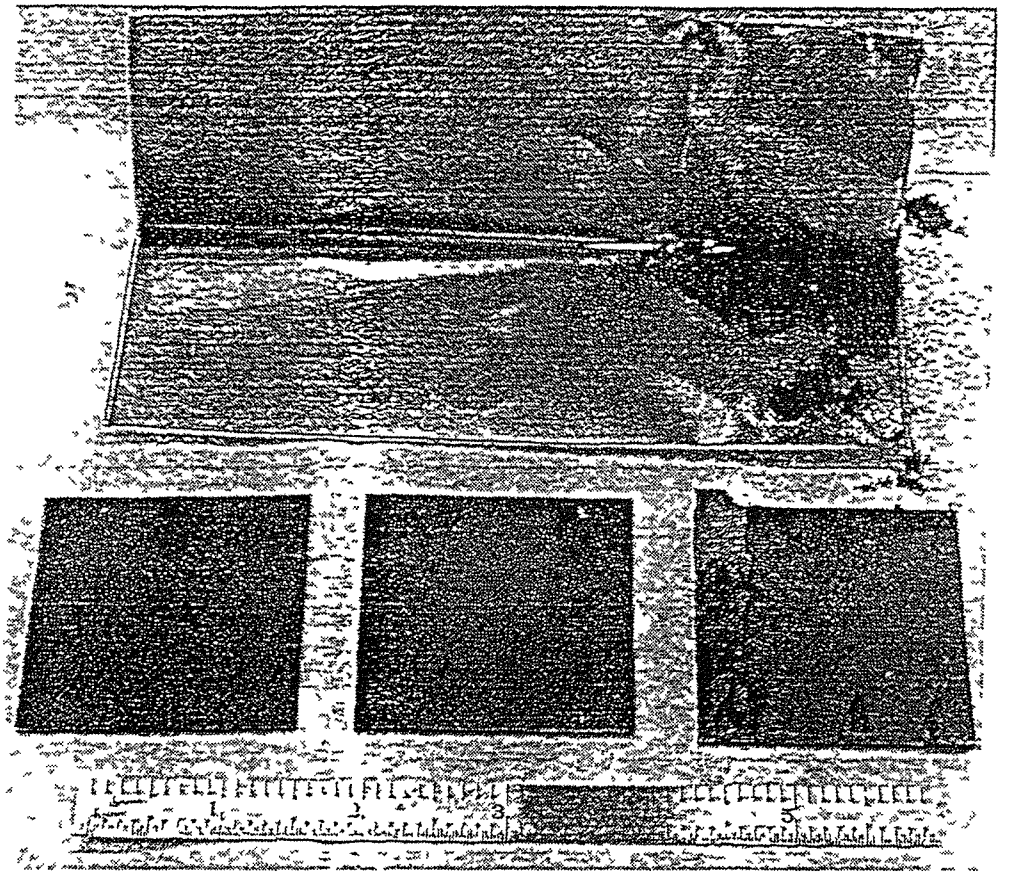

Figure 1-3. Declad ZPPR plate showing localized corrosion of right coupon

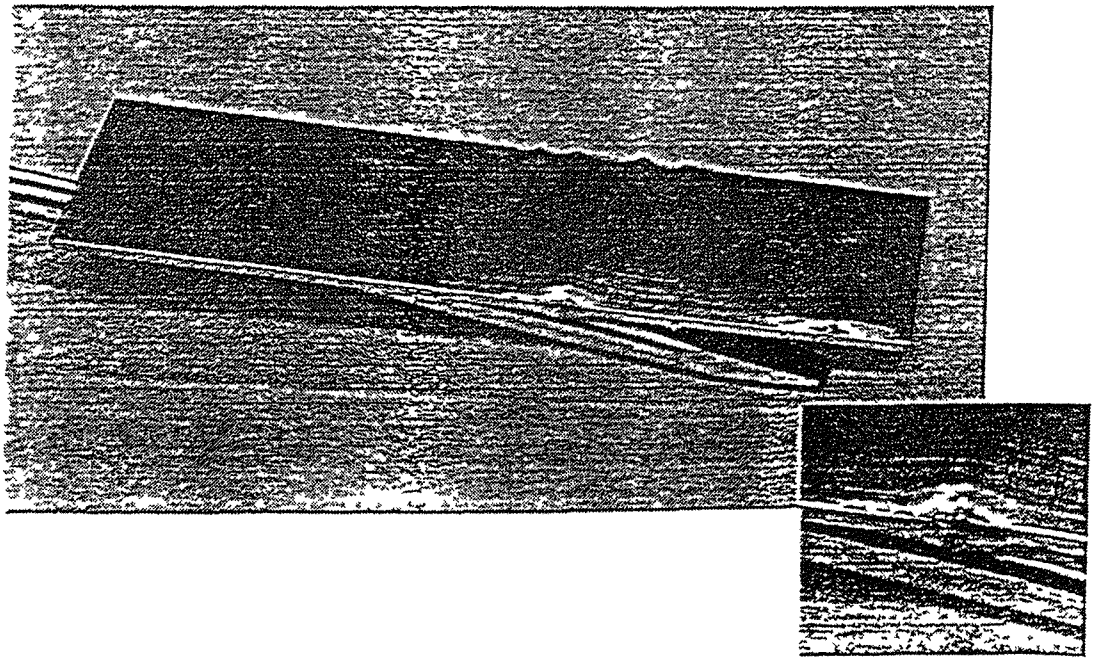

Figure 1-4 Bulged ZPPR plate, inset close-up of cladding breach

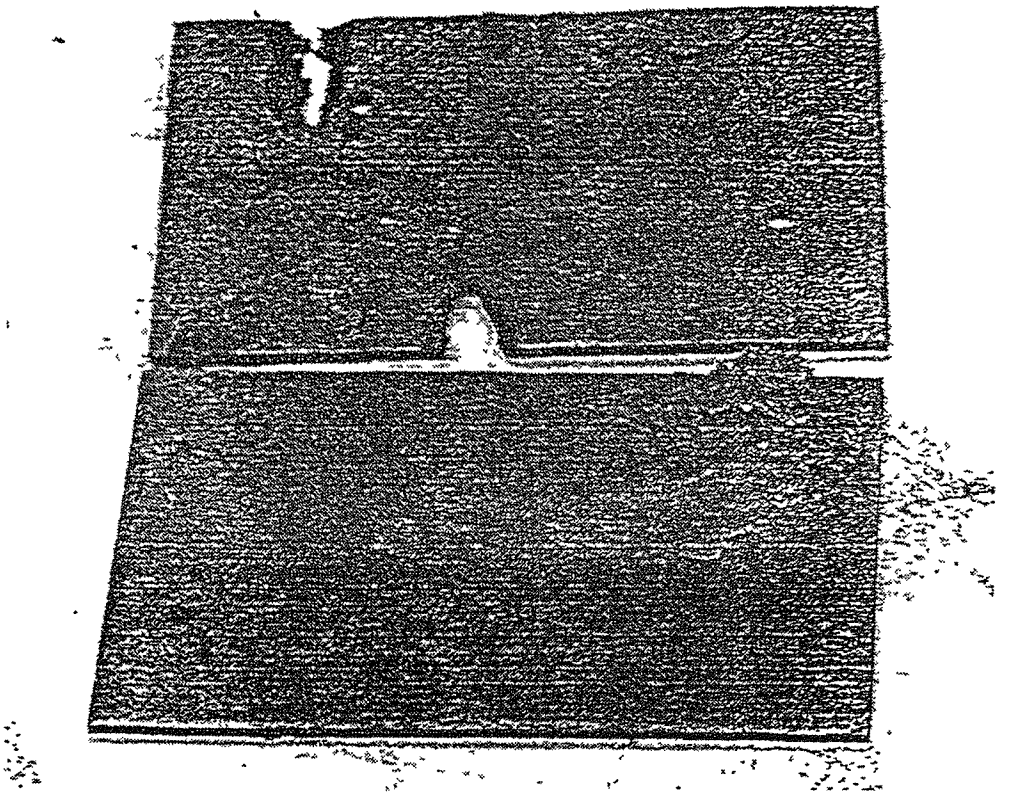

Figure 1-5 Coupons from plate in Fig 1-4 showing severe local and general corrosion.

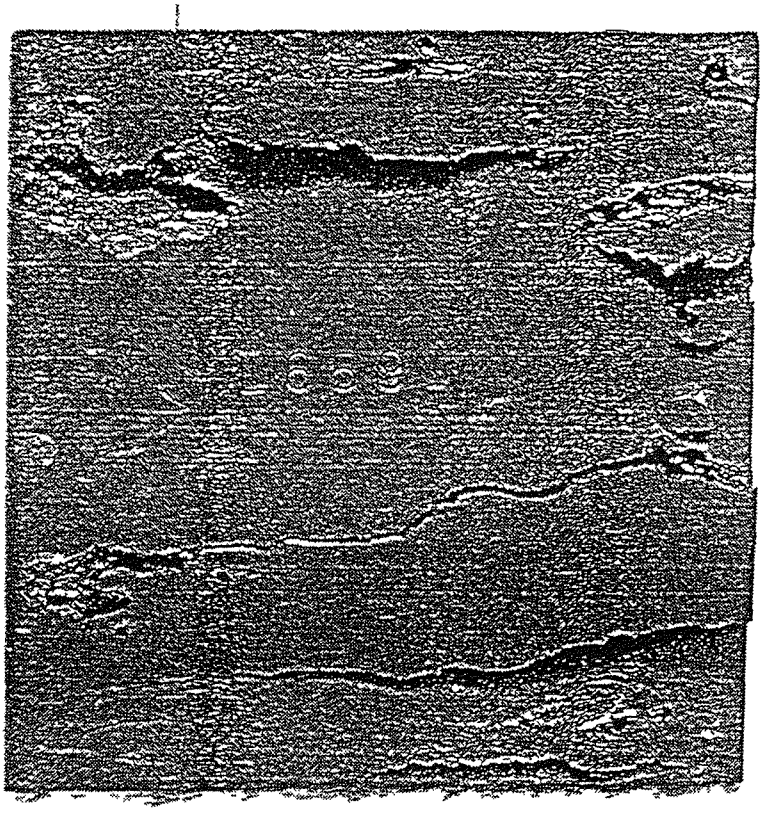

Figure 1-6. Coupon after removal of loose corrosion products showing severe localized corrosion.

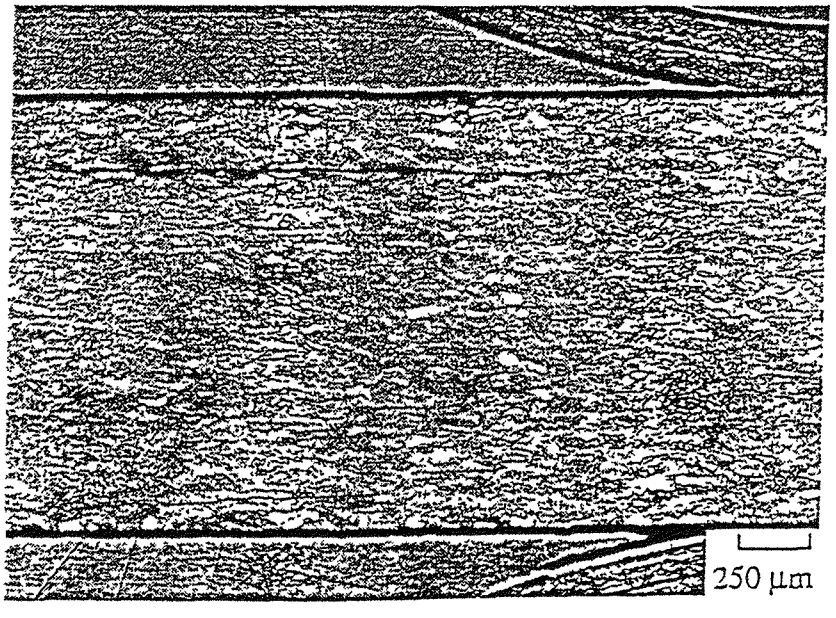

Figure 1-7 Metallographic cross-section of coupon from plate 3401 showing interior cracking and equiaxed grains (37 5X).

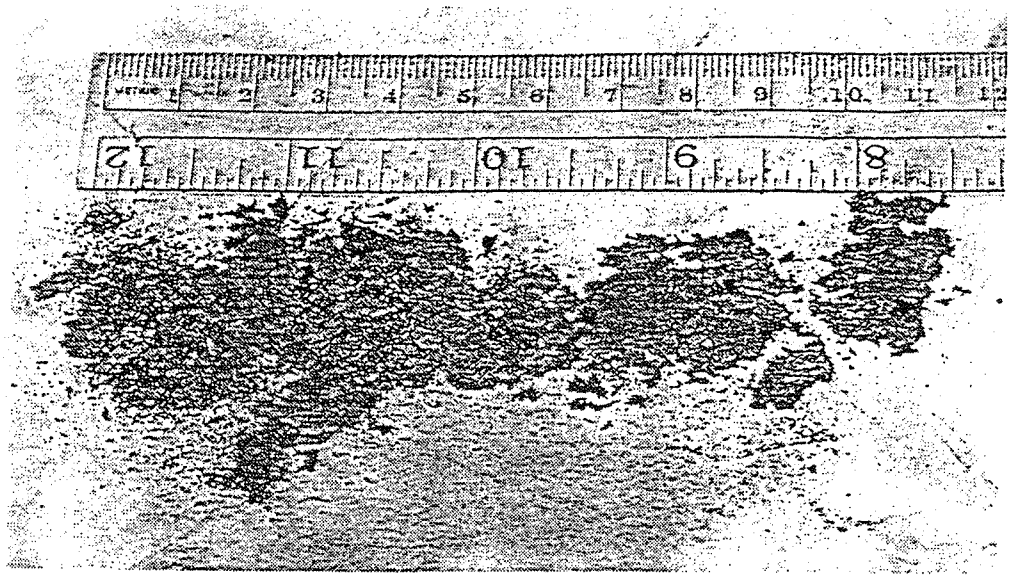

Figure 1-8. Loose flake and powder corrosion product from coupons shown in Fig. 1-5.

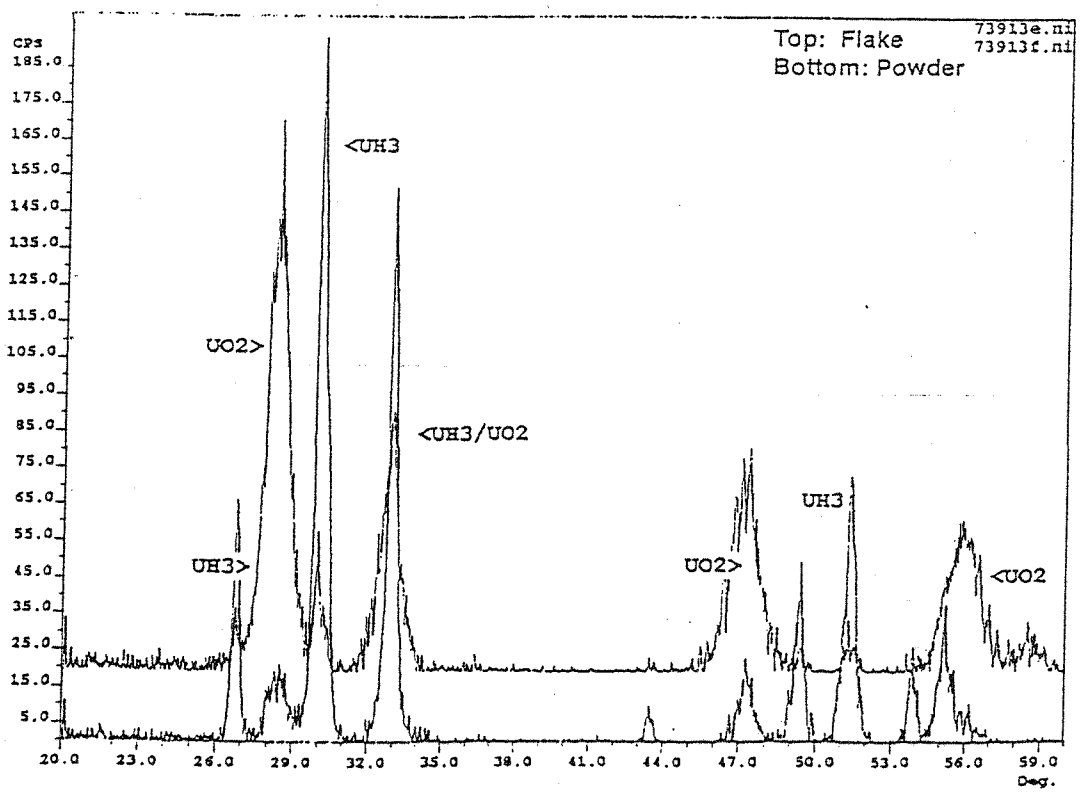

Figure 1-9. XRD patterns from flake and powder corrosion products.

PART 2
OXIDATION KINETICS OF ZPPR PLATE CORROSION PRODUCTS

I. INTRODUCTION

The previous part presented X-ray diffraction results and anecdotal evidence demonstrating that corrosion products from HEU ZPPR fuel plates contain significant quantities of UH_3, and that these corrosion products are reactive at room temperature when agitated. The results presented in this part provide a more quantitative measure of the hydride contents of the corrosion products, and the dependence of the oxidation kinetics of the corrosion products on oxygen concentration and temperature. Data of this nature will help provide a better technical basis for evaluating safety aspects of handling and drying corroded uranium fuels.

II. EXPERIMENTAL PROCEDURES

A. Testing Apparatus

Oxidation testing of the corrosion products was carried out using a modified Shimadzu TGA-51H thermo-gravimetric analyzer (TGA). The TGA is comprised of a Cahn-type microbalance to monitor weight changes, coupled with a resistance furnace to apply a temperature profile to the sample. Modifications to the Shimadzu instrument were made to allow operation of the instrument in a purified argon glovebox. The most significant changes were the connection of gas input and output lines to the TGA, and the construction of a gas control panel outside the glovebox. Both modifications were made to enable control of gas composition, flow rate, and pressure in the sample chamber. In addition, some electronic modifications were made to enable the use of a computer located outside the glovebox for TGA control and data acquisition.

The gas environment in the sample chamber is controlled by varying the rates of two separate gas flows which enter the chamber and the rate of exhaust flow out of the chamber. The first input flow is a pure Ar purge flow, which passes through the balance region of the TGA before entering the sample chamber. The second input flow contains a reaction gas, in this case a mixture of Ar and 30 vol.% O_2. The reaction gas flow enters the TGA just upstream of the sample chamber, and the two flows mix prior to entry into the sample chamber. The flow rates for the two streams are set using needle valves and flowmeters in the gas control panel outside the glovebox. The flowmeters are factory-calibrated and stated to be accurate to 5% of the flow rate reading.

Pressure in the chamber is measured by a pressure transducer in the outgas line just downstream of the TGA; the pressure is controlled by varying the exhaust flow rate using a booster pump - bypass valve combination in the exhaust line.

The resolution of the TGA microbalance is stated by the manufacturer to be 1 μg, with an accuracy of 1% of the measured value. The calibration of the TGA was checked by comparing weights of samples measured using a calibrated Satorious analytical balance with weights of the same samples measured using the TGA. Sample weights ranged from 17 to 268 mg; the weights obtained using the TGA agreed with the analytical balance weights to within 1% accuracy.

Measurement of the specific surface areas of the corrosion products was performed on a Quantachrome Quantasorb gas sorption analyzer using a technique based on the Brunauer, Emmett, and Teller (BET) theory of gas adsorption. No modifications to the instrument were made, however, due to the radioactive nature of the samples to be tested, the analyzer was located in a contaminated fume hood. Proper operation of the instrument was verified using TiO_2 and Al_2O_3 reference materials supplied by Quantasorb. The values measured using the Quantasorb tester agreed with the reported values (10 and 0.1 m^2/g, respectively) within 10%.

B. Testing Procedures

Three plates, serial numbers 3930, 3401, and 2962, were selected to obtain products for TGA and BET testing. The plates were chosen based on their apparent degree of corrosion, evidenced by bulging of the exterior stainless steel cladding. Plate 3930 had very little bulging, plate 3401 had an "average" amount of bulging, and plate 2962 had relatively severe bulging. These three plates were transferred into a pass-through Ar glovebox and de-clad. The atmosphere in the glovebox during the decladding procedure contained approximately 0.15% O_2. The corrosion product from each plate was examined. Contrary to indications from exterior appearance, plate 3401 contained the most loose corrosion product, 4.04 g. Plate 2962 contained 3.19 g, while plate 3930 contained 1.67 g. For the two more severely corroded plates (2962 and 3401), 0.01 g and 0.04 g samples of the flake-like product were removed from the corrosion products as a whole and placed into separate containers. The remainder of the products from the two plates were labeled "powder", although flake-like material was still present in the samples. After collection, the product samples from the three plates were transferred into a purified Ar glovebox for storage, loading of BET samples, and TGA testing.

Specific surface area measurements using the BET technique were performed on samples from all three plates. The BET testing matrix and results are shown in Table 2-1. Samples were loaded into standard sample cells in the purified Ar glovebox. The sample cells have quick-connect fittings which enable isolation of the sample from the ambient atmosphere until the cell is inserted into the analyzer for testing. Isolation of the sample prevented any reaction of the hydride with air once the cell was out of the glovebox. The loaded cells were transferred out of the glovebox to the contaminated fume hood and inserted into the analyzer. BET testing was performed using standard techniques with Kr gas as the adsorbate, He gas as the carrier, and N_2 gas for calibration. Adsorption was carried out at liquid nitrogen temperature. Three consecutive measurements were made on each sample. The sample cells were transferred back into the glovebox following testing.

TGA oxidation testing was performed on samples from plate 3401 only. All tests but one were performed on "powder" samples from this plate. One test was performed on a flake sample. Table 2-2 shows the testing matrix and results for the TGA tests. Samples for the TGA tests were obtained from powder located in the BET sample cell by simply pouring an appropriate amount from the BET cell into the TGA sample pan. No attempts were made to ensure that the samples were representative of the bulk powder.

Most tests were performed under "isothermal" conditions at temperatures ranging from 35°C to 250°C. For this type of test the TGA furnace was programmed to ramp up to the specified temperature and then maintain that temperature. During the heatup period, only pure Ar (purge gas) was flowing and present in the chamber. Once the test temperature was reached and stabilized, oxygen was admitted into the chamber by opening the reaction gas flow line. One test performed was of the "burning curve" type. For this test, the furnace was programmed to increase the temperature at a constant rate (15°C/min) until 800°C was reached. Both purge and reacting gas flows were on during the entire heatup period. All tests were performed at a nominal pressure of 10 psi absolute, and with 200 ml/min total gas flow.

Sample weight and furnace temperature data from the TGA were acquired and logged by the control and data acquisition software. Data was typically acquired every second, but for longer-term tests data was acquired every ten or fifteen seconds in order to minimize file sizes. Plots of weight gain versus time were produced using Kaleidagraph software. These plots were analyzed to determine rates of reaction using the same software.

After TGA testing, all samples were visually examined for discernible changes in appearance due to oxidation. Two samples (from tests ZPPR4 and ZPPR13) were sent to the

Analytical Laboratory for XRD analysis. XRD was used to qualitatively determine the products of the reaction of the powder with oxygen.

III. RESULTS AND DISCUSSION

A. Specific Surface Areas of Corrosion Product Powders

Table 2-1 shows sample weights, surface areas, and specific surface areas for corrosion product samples from the three ZPPR plates. The data points shown for surface area and specific surface area are based on an average of three consecutive tests on each sample. The results for "powders" were fairly consistent, varying from 0.75 to 1.01 m^2/g for the three samples tested. The test of the 3401 flake material shows that its specific area (0.66 m^2/g) is very similar to that of the powder material. However, the small sample size (0.097 g), and hence desorption signal, reduces the confidence in this value. A second test on flake material with a much larger sample size is planned. The values obtained for both powder and flake lie within those reported in the literature for UH_3, 0.3 to 0.6 m^2/g by Longhurst [1], and 2.8 m^2/g by Stakebake [2].

B. Oxidation Kinetics of Plate 3401 Product

Table 2-2 shows a summary of all TGA oxidation tests performed on samples from plate 3401, both powder and flake. The tests fall into two groups – those which showed "ignition" behavior, and those which slowly oxidized. Ignition of a sample was indicated by a high rate of weight increase and a corresponding increase in furnace control thermocouple temperature. Ignition occurred for test temperatures of 150°C and above, with the exception of one test discussed below.

The weight gain as a function of time during ignition and burning of samples had a sigmoidal shape, as shown in Fig. 2-1 for ZPPR4A. The rate of weight gain quickly increased at the beginning of the test to a fairly linear rate. The rate decreased near the completion of oxidation, finally dropping to zero when the sample was consumed. Burning rates corresponding to the central linear portion of the weight gain versus time curve are reported in Table 2-2. The burning rates observed at both 9% and 20% O_2 were consistent and, more importantly, were independent of sample size or test temperature. Burning rates in Ar - 9% O_2 varied from 0.051 mg/sec to 0.073 mg/sec; rates in Ar - 20% O_2 varied from 0.095 mg/sec to 0.141 mg/sec. The lack of dependence on sample size (and hence surface area) and temperature led to the preliminary conclusion that the burning rate was limited by mass transport in the gas phase. This assertion was corroborated by

the fact that burning rates were lower for 9% oxygen concentration in the gas compared to 20% concentration.

The total weight gains of samples after completion of burning were used to calculate the weight fraction of UH_3 in the sample. For tests in which ignition did not occur, a second run, denoted with the suffix "A", was run on the same sample at a higher temperature to ignite the sample and so measure the total weight gain. In order to calculate the UH_3 fraction, the stoichiometry of the oxide formed in the burning reaction needed to be known. For this reason XRD analyses of reaction products from two tests were performed. Unfortunately, the results of this analysis were not conclusive. The XRD patterns showed peaks which could correspond to several different oxides, including UO_2, U_3O_7, U_3O_8, and UO_3. There was extensive peak overlap and broadening, which prohibited quantitative determination of the relative fractions of the various oxides. To enable a calculation of hydride fractions, all oxide produced by burning was assumed to be U_3O_8. This oxide had a good fit with the patterns obtained, and also represents an average stoichiometry for the various possible oxides.

The actual calculation was performed as follows. The weight gain of one gram of UH_3 oxidizing to U_3O_8 ($UO_{8/3}$) according to the reaction

$$UH_3 + 4/3\ O_2 \rightarrow UO_{8/3} + 3/2\ H_2 \qquad (2\text{-}1)$$

was calculated to be 0.168 g. The weight fraction of UH_3 is then given by:

$$\%UH_3 = \frac{\text{wt. gain (g)}}{0.168 \times \text{ sample wt. (g)}} \qquad (2\text{-}2)$$

The calculated hydride fractions for plate 3401 powder samples varied from 47 to 61 wt.%. The hydride fractions for the "powder" material do represent the bulk loose product as a whole, since the "powder" material also contained nearly all of the flake found in the plate. Of the four grams of product, only 0.1 g of flake was removed for separate testing. The remainder of the product was designated "powder". It must be noted, however, that the measured fractions do not take into account the adherent product that was not removed from the plates. Due to this adherent nature, this product is believed to be mainly oxide, and therefore the actual fraction of hydride in the corrosion product as a whole is expected to be less than the measured values for the loose product. For comparison, the fraction of hydride which can be formed during uranium corrosion by water,

assuming full recycling of hydrogen, is 57 wt.%. Hence the observed hydride fractions are a significant fraction of the theoretical maximum for the water reaction.

The hydride fraction of each sample was used to calculate the reactive surface area of that sample. The reactive surface area was calculated as the product of the mass of the sample, the specific surface area of the material, and the fraction of hydride in the sample. The reactive surface area was used to calculate surface area normalized rate data for all tests. Because the burning rate data was independent of sample size, normalizing the burning rate data by surface area only increased the scatter in the data. Hence burning rates are reported in units of mg/sec. Obviously, the independence of burning rate on sample size is only valid for the range of sample sizes tested, 50 to 200 mg. Further tests on small samples are planned in an attempt to determine a surface area dependent burning rate. The low-temperature oxidation rates were assumed to be surface area dependent.

The results of the one test on plate 3401 powder which was run in a burning curve mode are shown in Figure 2-2, which shows both the weight gain of the sample and the furnace control thermocouple reading as a function of test time. The control thermocouple was located approximately 2 mm below the Pt sample pan containing the sample. The sharp break in the weight gain curve at approximately 142°C clearly corresponds to the onset of ignition. There is a matching increase in the control thermocouple reading resulting from rapid heat generation in the sample. Similar increases in control thermocouple readings were also observed for isothermal tests in which ignition occurred. The post-ignition burning rate of the burning curve sample was the same as observed in isothermal tests.

Test ZPPR16 was the one run at 150°C in which ignition did not occur. The sample size for the test was very small, only 18.4 mg. This amount of powder was not sufficient to form a powder bed in the sample pan, unlike larger samples. The powder particles were scattered loosely on the bottom of the pan. Heat conduction away from such a sample will be much greater than for a powder bed. It is postulated that high heat conduction raised the ignition temperature for this sample above 150°C. Further testing is planned to investigate the effect of sample size on ignition temperature for this material.

Oxidation of plate 3401 powder at conditions for which ignition did not occur was characterized by a decreasing rate of oxidation with increasing test time. Figure 2-3 shows a typical low-temperature oxidation curve. For the first several tests at lower temperature, it was thought that the rate of oxidation became linear after a short period of time, and so these tests were

run only long enough to obtain what appeared to be a linear rate. Further testing, however, revealed that the rates did not become linear but continued to slowly decrease with test time. Decreasing rate kinetics are typically described as being parabolic or "paralinear" (a combination of parabolic and linear kinetics). Attempts to fit the low temperature data with rate laws corresponding to parabolic or paralinear kinetics were unsuccessful, as was the more general approach of fitting a power law relationship to the data. Some rate laws fit the data for certain tests better than others, but no single rate law adequately described all tests.

In order to make quantitative comparisons between tests at different temperatures (and so determine an activation energy), average rates for the various tests were computed. The average rates were calculated by dividing the total weight gain at a given time by the time. Due to the decreasing oxidation rates, the average rates decreased with increasing time. For this series of tests, average rates in two time regimes were computed—a short time regime and a long time regime. For tests with durations less than 100 min, the short time average rates were computed as the weight gain at end-of-test divided by total test time. The short time average rates for tests with durations greater than 100 min were computed as the weight gain at 100 min divided by 100 min. Similarly, the long time average rates for tests with durations between 100 min and 300 min were computed as the weight gain at end-of-test divided by total test time, while the rates for tests longer than 300 min were computed as the weight gain at 300 min divided by 300 min. As mentioned above, the oxidation rates for all low-temperature tests were surface area normalized.

The rate of oxidation below the ignition temperature generally increased with increasing testing temperature. Figure 2-4 is a summary plot showing weight gain as a function of time for longer-duration tests in Ar-20%O_2. With the exception of the 35°C and 60°C tests, the rate of oxidation increases with increasing temperature. It is believed that rates of oxidation at the two lowest temperatures may have been sufficiently low that normal drift in the TGA baseline reading over time may have obscured the real weight gain.

Figure 2-5 is an Arrhenius plot of the low-temperature oxidation rates. The short time average rates for Ar-9%O_2 and Ar-20%O_2 are shown along with the long time average rates for Ar-20%O_2. There is considerable scatter in the data; the data for the different time averages and oxygen concentrations are not significantly different in comparison with this scatter. A straight line fit to the log rate versus inverse temperature plot yields the following rate equation for oxidation of plate 3401 powder in Ar-9%O_2 and Ar-20%O_2:

$$k = 2\text{x}10^{-2} \exp\left[\frac{-\Delta G}{RT}\right] \text{mg/cm}^2\text{/sec} \qquad (2\text{-}3)$$

with

$$W = k\,t \qquad (2\text{-}4)$$

$$\Delta G = 36 \pm 6 \text{ kJ/mol} \qquad (2\text{-}5)$$

where W is the weight gain of the sample, k is the rate constant, and t is time.

The results from the test performed on the flake sample from plate 3401 (ZPPR7) showed that there was no significant quantity of hydride associated with this sample. The weight change over a 15 min period at 150 °C was 0.01 mg. All powder samples showed very significant weight changes—either burning or fairly rapid oxidation—over a similar time period. The flake sample was visually unchanged after testing. The stability of the flake material was also evidenced by its behavior in powder tests. Because not all flake was separated from the plate 3401 corrosion product, some flake material was present in the nominally "powder" samples. This flake remained visually unchanged following oxidation or ignition of the sample, unlike the powder, which experienced an increase in volume due to oxidation.

The data obtained in this series of tests compares somewhat favorably with the limited amount of information available in the literature. Both Longhurst [1] and Stakebake [2] have performed oxidation tests with uranium hydride. Longhurst reported that little or no reaction occurred at room temperature (possibly due to oxide impurities), but observed ignition at 140°C, which is very close to the value of 142°C obtained in this series of tests. The rates reported by Stakebake at temperatures between 0°C and 100°C appear to match well with the burning rates observed for plate 3401 powder in Ar-20%O_2, approximately 0.1 mg/sec of weight gain. The temperatures at which these rates occurred were much lower than in this series of tests, indicating that ignition occurred at lower temperatures. The lower ignition temperature could be due to a higher specific surface area (2.8 m^2/g) for Stakebake's hydride material, or less oxygen contamination present on the hydride.

The low temperature oxidation rates are comparable to oxidation rates for uranium metal in dry air published in a review by Ritchie [3]. Figure 2-6 shows the rates for uranium metal and those for the current tests. One apparent difference in the data is a lower activation energy (slope) for uranium hydride oxidation compared to uranium metal oxidation. The reason for this difference is unknown.

IV. FURTHER TESTING

Further testing of ZPPR fuel corrosion products will concentrate on several areas. First, samples from additional plates will be tested to determine the extent of plate-to-plate variations in oxidation kinetics and hydride content, and also to assess any effects of corrosion extent on corrosion product properties. Second, oxidation and burning rate data are needed at lower oxygen concentrations. Tests will be performed at 4% and 1% oxygen content to obtain this data. Third, additional data is needed on the flake material to substantiate the initial findings that it is inert uranium oxide, and to obtain a second surface area measurement.

V. CONCLUSIONS

Initial testing of the corrosion products found on uranium metal ZPPR fuel plates was performed. Characterization of the products included specific surface area determination and measurement of oxidation kinetics in Ar-20%O_2 and Ar-9%O_2. The following conclusions were reached:

- The specific surface areas for loose corrosion product powders varied from 0.75 m^2/g to 1.01 m^2/g. The specific surface area for flake material, measured in one test, was 0.66 m^2/g.
- TGA oxidation testing of product material from one plate showed that the ignition temperature for 50-200 mg samples of the product was between 125°C and 150°C.
- Burning rates above the ignition temperature were independent of sample size in the range of 50-200 mg; the average burning rate in Ar-20%O_2 was 0.1 mg/sec.
- Oxidation rates below the ignition temperature decreased with increasing test time. No single rate law described the behavior of all tests. The average oxidation rates were described by the following equation:

$$k = 2\text{x}10^{-2} \exp\left[\frac{-36\ \text{kJ/mol}}{RT}\right] \text{mg/cm}^2\text{/sec} \qquad (2\text{-}6)$$

- The calculated hydride fractions in the loose corrosion product from ZPPR plate 3401 varied from 47 to 61 wt.%.
- The flake material from plate 3401 did not significantly react at 150°C.

REFERENCES

[1] G.R. Longhurst, Pyrophoricity of Tritium-Storage Bed Materials, EG&G Idaho Report EGG-FSP-8050 (1988).

[2] J.L. Stakebake, in Chemistry Research and Development – Research and Development Semi Annual Progress Report, January-June 1977, Rocky Flats Report RFP-2680 (1977).

[3] A.G. Ritchie, J. Nucl. Mater. 102 (1981) 170.

Table 2-1. BET Results Summary

Material	Sample Weight	Surface Area	Specific Surface Area
3401 Powder	0.827 g	0.62 m^2	0.75 m^2/g
3401 Powder	3.074 g	2.3 m^2	0.76 m^2/g
3401 Flake	0.097 g	0.065 m^2	0.66 m^2/g
2962 Powder	2.107 g	2.1 m^2	1.01 m^2/g
3930 Product	1.563 g	1.2 m^2	0.76 m^2/g

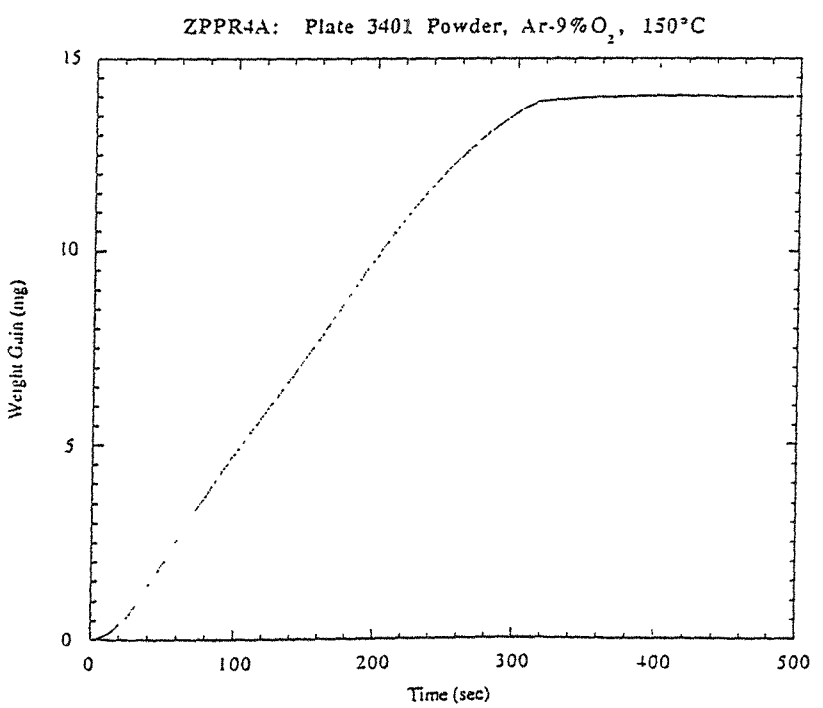

Figure 2-1. Typical weight gain versus time plot for burning of plate 3401 powder.

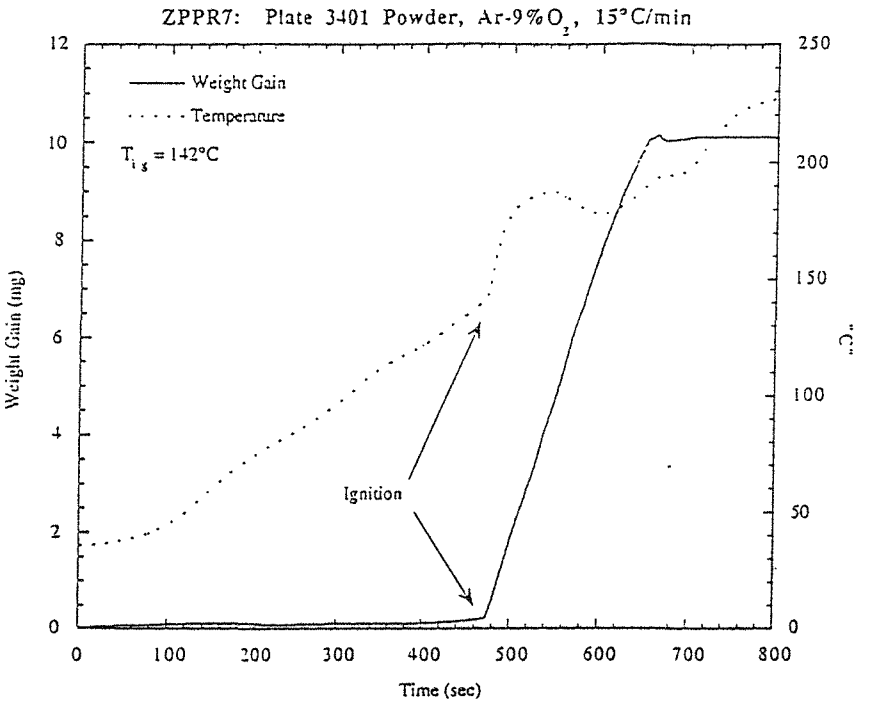

Figure 2-2. Plot of weight gain and control thermocouple temperature for burning curve test.

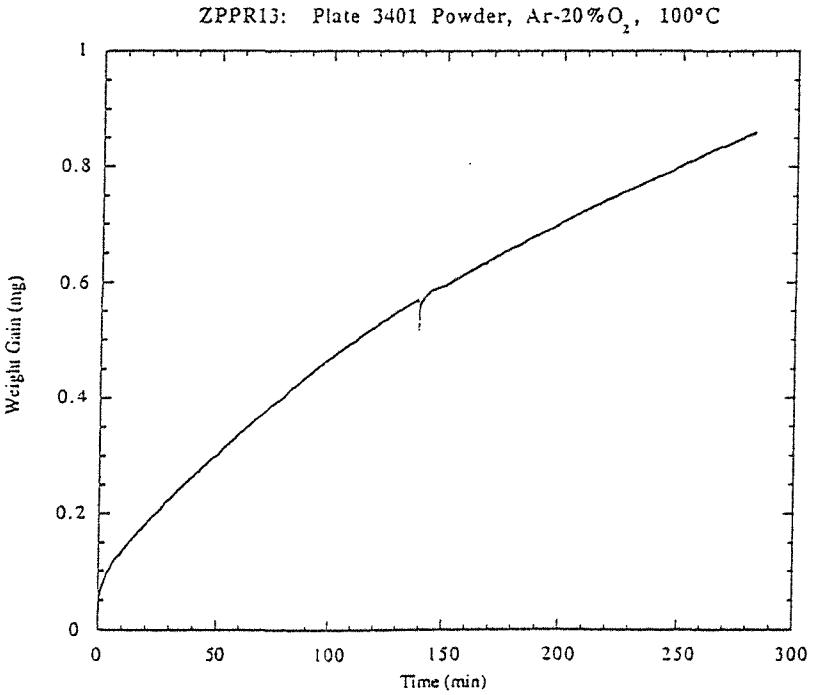

Figure 2-3. Typical weight gain versus time plot for low-temperature oxidation of plate 3401 powder.

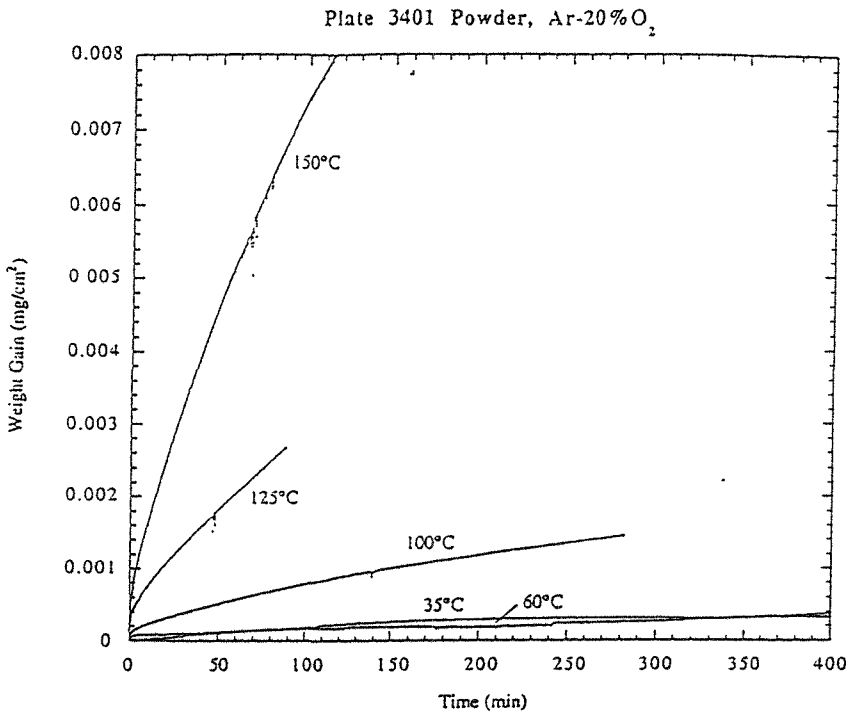

Figure 2-4. Plot of weight gain versus time for longer-duration tests in Ar-20%O_2.

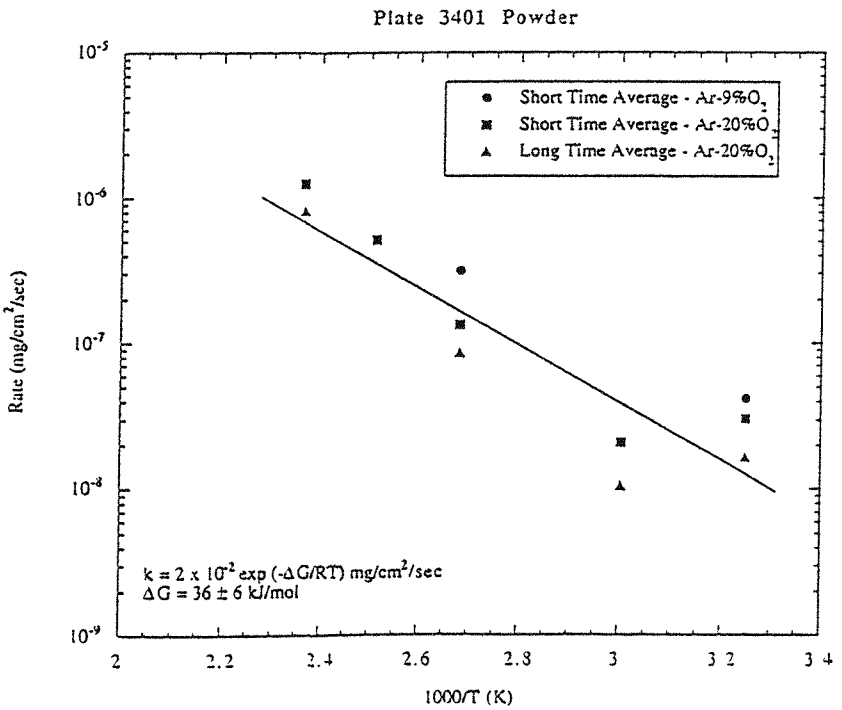

Figure 2-5. Low-temperature oxidation rates versus reciprocal temperature.

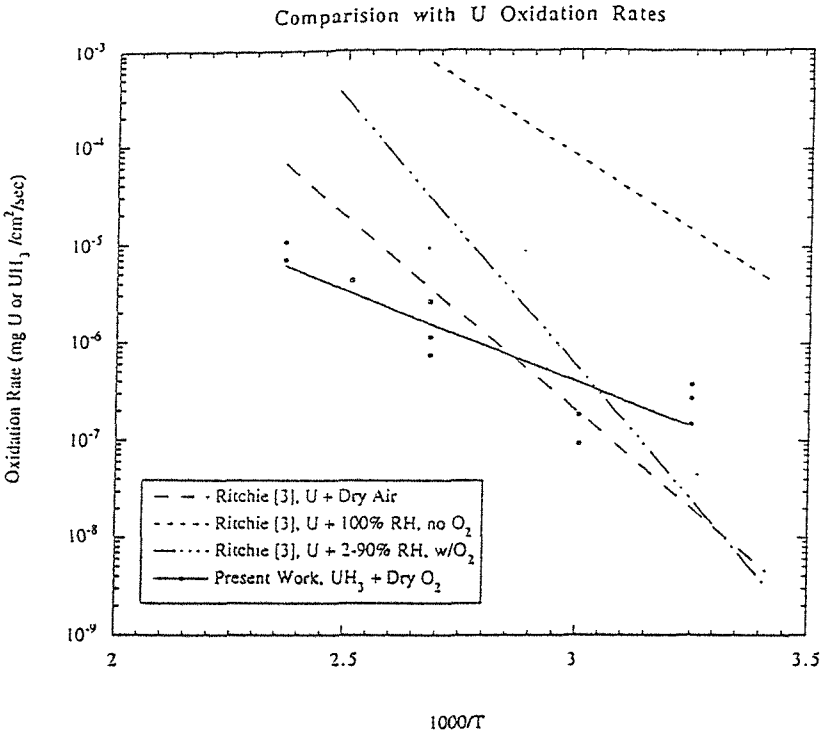

Figure 2-6. Comparison with U oxidation data from Ritchie [3].

Distribution for ANL-98/11

Internal:

D. C. Crawford
S. M. Frank (5)
S. L. Hayes (5)
J. R. Krsul
H. F. McFarlane
D. N. Olsen
R. G. Pahl (5)
D. L. Porter
C. W. Solbrig
T. C. Totemeier (5)
L. C. Walters
TIS Files

External:

DOE-OSTI (2)
ANL-E Library
ANL-W Library
Manager, Chicago Operations Office, DOE